ORIGINAL PAPER

Role of Ho Doping in Magnetization Mechanism of BiFeO$_3$ Thin Films

Yuhan Wang[1] · Yanjie Wang[2] · Maobin Wei[3] · Junkai Zhang[3] · Yilin Zhang[3]

Abstract

BiFeO$_3$ (BFO) as one of the considerable interesting multiferroic materials has been widely investigated for its fantastic science and potential application. Herein, effects of Ho doping on the structure, morphology, and magnetic properties of BFO thin films were systematically studied. X-ray diffraction (XRD) indicates a successful substitution of Ho at Bi site and a transition in crystal structure of Bi$_{0.9}$Ho$_{0.1}$FeO$_3$ (BHFO) thin film. Raman scattering spectrum is further evidence of XRD analysis results. The Ho-doped BFO thin films possess uniform morphology. X-ray photoelectron spectroscopy (XPS) confirms that the substitution of Bi^{3+} ions with Ho^{3+} ions is beneficial. The remanent magnetization of BHFO thin films is about three times than that of the BFO thin films under a maximum magnetic field of 15,000 Oe. And we systematically discussed several possible reasons for the enhancement of magnetization.

Keywords BiFeO$_3$ · Multiferroic · Substitution · Crystal structure · Magnetization

1 Introduction

Multiferroic materials simultaneously exhibit a variety of ferrous properties like ferroelasticity, ferroelectricity, and ferromagnetism [1–4]. BFO is known to be one of several so-called multiferroics since it can show a high Curie temperature (TC~1103 K) and the Neel temperature (TN~643 K) above room temperature [5–7]. The multiferroic property of BFO makes it a promising possibility in novel storage media and spintronic devices. At ambient conditions, BFO crystallizes in a rhombohedral-distorted perovskite structure with space group R3c at room temperature [8–10]. Although significant progress had been made in the development of BFO, some issues related to the fundamental properties for this system require further investigation [11–13]. BFO has a G-type antiferromagnetic structure, and this modulated spin-cycloidal structure inhibits the observation of total magnetization [14–17]. The researchers have taken many methods to destroy the modulated spin structure, such as substituting rare earth element for A site by a different radius of ions [18] and preparing a thin film on different substrates [19]. Zheng et al. reported that the maximum value of Ms. in BFO thin film doped with Er^{3+} ions at a concentration of 0.09 is 2.60 emu/cm^3 [20]. Furthermore, Jesús et al. reported when the doping concentration of Ni is 0.1, the value of Ms. is at most 2.9 emu/g [21]. Mukherjee et al. reported the enhancement of magnetization (0.21–9.24 emu/g) of the BFO nanoparticles may be regarded as the presence of impurity phases, temperature dependence, and increase of Co content [22]. Among various kinds of element reported at A site in BFO, Ho^{3+} ions are expected to improve magnetic properties, due to the exchange interaction between the 4f electron of Ho^{3+} ion and 3d electron of Fe^{3+} ion. Ho^{3+} ions are magnetically active ions with large magnetic moments. The ferromagnetic coupling between Ho^{3+} and Fe^{3+} ions can increase the magnetization value compared with other non-magnetic rare earth-doped systems [23]. In order to improve the magnetic properties of BFO, many scientific research teams have studied the synthesis of BFO and its base materials extensively. The replacement of Ho is expected to have a positive impact on the future application of specific multifunctional devices. Therefore, it is still a meaningful subject to improve its magnetic properties.

In our paper, we report the effect on magnetism of structural distortion caused by Ho^{3+} ions (ion radius 1.015 Å)

✉ Yilin Zhang
yl4568520@126.com

1 State Key Laboratory of Inorganic Synthesis and Preparative Chemistry, Jilin University, Changchun 130012, People's Republic of China

2 Key Laboratory of Physics and Technology for Advanced Batteries (Ministry of Education), Department of Physics, Jilin University, Changchun 130012, China

3 Jilin Normal University, Changchun 130013, People's Republic of China

doping BFO thin film synthesized by the sol–gel methodology. Certain significant ferromagnetic properties have been observed at room temperature, and the local structural distortion has been caused by Ho^{3+} ion doping.

2 Experimental Details

2.1 Materials Preparation

The BFO and BHFO thin films were prepared by a simple sol–gel method. A conventional sol–gel spin-coating process was utilized for the synthesis of all thin films. Firstly, appropriate proportions of $Bi(NO_3)_3 \cdot 5H_2O$ and $Fe(NO_3)_3 \cdot 9H_2O$ were used as starting materials for BFO thin films and were dissolved together in ethylene glycol. The mixture was stirred at room temperature for 6 h until a homogenous BFO precursor solution was obtained. Then, this precursor solution was deposited onto clean Si (100) substrates and then were preheated at 350 °C for 6 min to remove solvent. These above processes were repeated 8 times. After that, the BFO thin films were heat-treated at 500 °C for 1 h. Secondly, appropriate proportions of $Ho(NO_3)_3 \cdot 5H_2O$, $Fe(NO_3)_3 \cdot 9H_2O$, and $Bi(NO_3)_3 \cdot 5H_2O$ were used as starting materials for BHFO thin films. The subsequent experimental process and condition of the parameters were same as the previous description.

2.2 Characterization

The crystalline structure characterizations of all thin films were checked up by X-ray diffraction (XRD) on a Rigaku D/Max 3C. Raman spectra of all samples were measured in backscattering geometry using a Renishaw Micro Raman spectrometer with a monochromatic radiation of $\lambda = 532$ nm. The morphology of BFO and BHFO thin films were performed by a scanning electron microscope (SEM, Model Hitachi, S-570) and a transmission electron microscope (TEM, 200 keV, JEM-2100HR, JEOL Ltd., Tokyo, Japan). Magnetic hysteresis (M-H) loops were generated by a Lake Shore 7407 vibrating sample magnetometer (VSM, Lake Shore, Columbus, OH, USA). And the chemical states of all thin films were measured via an ESCALAB 250XI X-ray photoelectron spectrometer (XPS, Thermo Fisher Scientific, Waltham, MA, USA).

3 Results and Discussion

3.1 Structural and Morphology Characterizations

The XRD patterns of the BFO and BHFO thin films deposited on the Si substrates are shown in Fig. 1. All diffraction patterns of all thin films are indexed to a rhombohedral
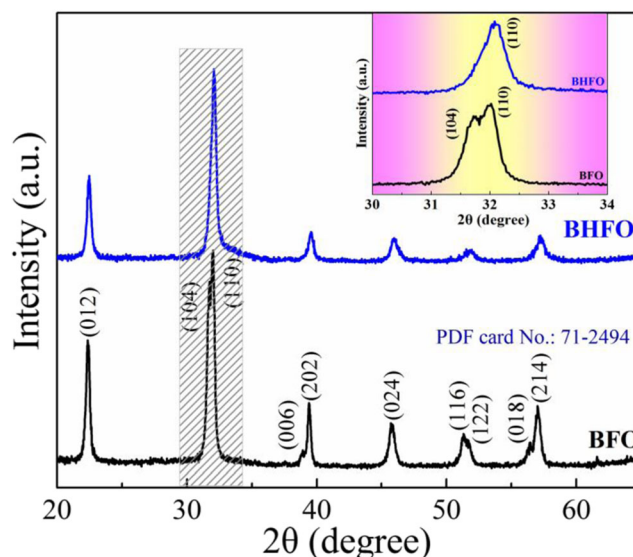
Fig. 1 X-ray diffraction spectra of the BFO and BHFO thin films with the inset of magnified patterns showing diffraction at around 32°

perovskite structure according to the JCPDS file card no. 71-2429 without any secondary phases. The inset of Fig. 1 shows an enlarged view of the XRD pattern of (104) and (110) at around 32°, where the peaks shift to higher angles and form a broadened peak, indicating that the lattice parameters transform after Ho doping [24]. This transformation can be attributed to the substitute of the smaller Ho^{3+} (ionic radius 1.015 Å) at the Bi (ionic radius 1.20 Å) site. This transformation confirms that Ho^{3+} ions probably occupy Bi sites in BFO thin films. This may have an effect on the magnetization of BHFO thin films. The crystal structure parameters of BHFO and BFO thin films are summarized in Table 1, which are determined from Bragg's law:

$$2d\sin\theta = n\lambda \tag{1}$$

And the crystallite sizes (D) are estimated from XRD patterns by Scherrer's formula:

$$D = \frac{K\lambda}{\beta\cos\theta} \tag{2}$$

where D, λ, K, β, θ is the particle size, the Cu k_α radiation wavelength of the X-ray, and the shape factor (taken as 0.9), the FWHM of the peak being considered and half of the

**Table 1** Crystal structure parameters and grain sizes of BFO and BHFO thin films

Samples	$a = b$ (Å)	c (Å)	V (Å^3)	Grain size (nm)
BFO	5.596	6.916	187.55	18.4
$BH_{0.1}FO$	5.601	6.846	185.98	17.8

Fig. 2 (a, b) Low magnification TEM images of BFO and BHFO thin films and the insets in (a, b) show high resolution TEM images of all thin films
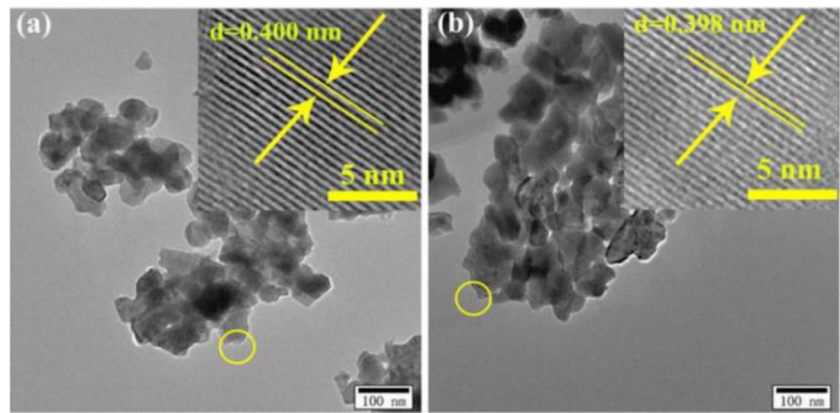

Fig. 3 SEM surface (a, b) and cross-sectional (c, d) images of the BFO and BHFO, respectively
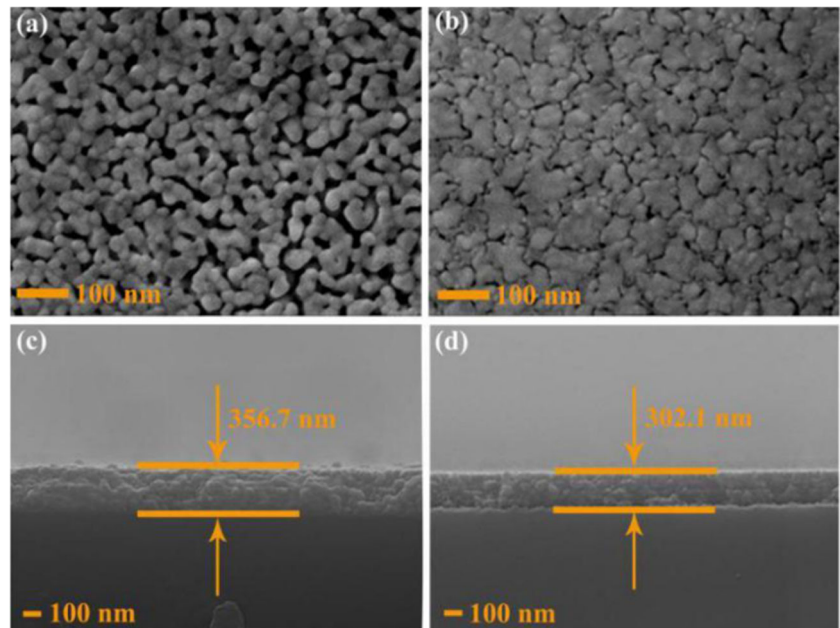
diffraction angle, respectively. As is clear from Table 1, lattice parameters and the volumes of the original unit cell are reduced by Ho substitution. This further proves the fact that the Ho substitutes Bi site. Raman spectroscopy (Fig. 3) and XPS (Fig. 5) provide additional supporting evidence.

Figure 2 a and b show the TEM micrographs which can be used to observe the detailed morphology of BFO and BHFO thin film. With the substitution of the Ho^{3+} ions, the grain sizes seem to decrease slightly. Illustrations of HRTEM images from Fig. 2(a, b) are shown in the circular area. These pictures indicate typical crystalline regions of 0.400 nm and 0.398 nm, which correspond to the (012) plane of the BFO thin films.

In order to shed more light on the influence of each specimen, we exhibit the SEM photos of BFO and BHFO thin films. Figure 3 a and b depict the surface morphology of BFO and BHFO thin films. From this spectrum, one can
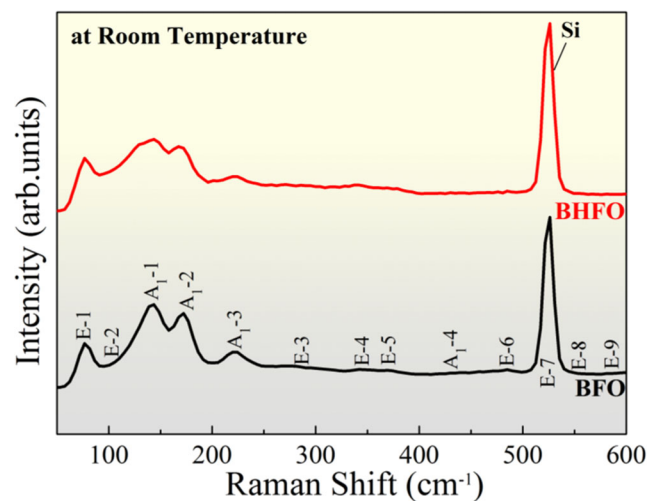

Fig. 4 Raman spectra of the BFO and BHFO thin films under the excitation line of 532 nm at room temperature

see that BHFO exhibits more uniform morphology compared with BFO thin film. This situation indicates that Ho doping is conducive in reducing the surface heterogeneity of the film [25]. The cross-sectional images shown in Fig. 3 c and d are specially obtained by means of scratching thin films. From the images, we can see that the BFO and BHFO thin films are well adhered to the Si wafers. In addition, the thicknesses of all thin films detected from the figures are about 356.7 and 302.1 nm, respectively.

3.2 Raman Scattering

Raman spectroscopy is a forceful means to confirm the structure and vibration behaviors of the materials. Figure 4 shows the Raman spectroscopy of the BFO and BHFO thin films measured in the range of 50–600 cm^{-1}. Three strong scattering peaks can be observed at 141.3, 170.7, and 221.8 cm^{-1} in the BFO thin film, which is consistent with those of the BFO thin films in other
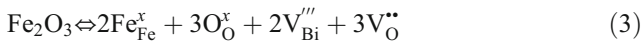
Fig. 5 (a) Overall core level X-ray photoelectron spectra for the BHFO thin film at room temperature. (b, c, d, e) XPS spectra of Bi 4f, Fe 2p, O 1s, and Ho 4d
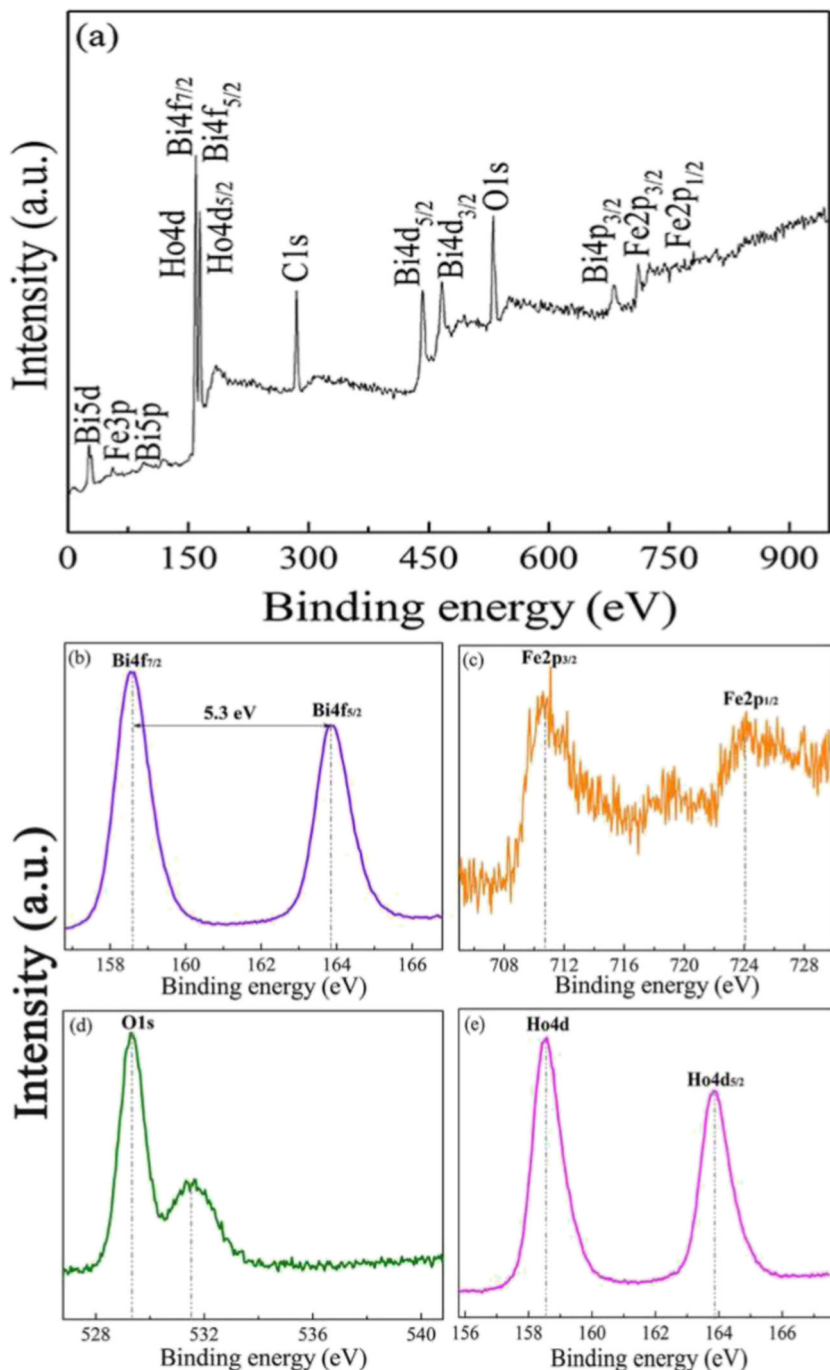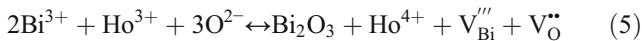
literature [26, 27]. The three regions have been proved for the Bi–O vibrations. The intensity of the A_1-1, A_1-2, and A_1-3 peaks in the BHFO thin film is lower than that of the BFO thin film. Moreover, the peak is broadened at 170.7 cm^{-1}. Yuan et al. [28] revealed that the stereochemical activity of the Bi6s^2 lone pairs plays an important role in the variety of Bi–O bonds. Therefore, the decrease of the intensity and the increase of the width in the Raman peak are regarded as the doping of Bi^{3+} ion via Ho of A site, which results in a decline in the stereochemical activity of BHFO thin films [29]. Raman results further demonstrate that Ho has entered Bi sites.

3.3 XPS Analysis of the BHFO Thin Films

To identify the chemical bonding and the role of Ho doping on the magnetic behaviors of BFO thin films, we performed the XPS measurements of the BHFO thin films. Figure 5 a reveals the full-scan spectrum of BHFO thin films. Figure 5b–d show the photoemission peak for Bi 4f, Fe 2p, O 1 s, and Ho 4d. The peaks at 163.9 and 158.6 eV are predominantly due to Bi 4f$_{5/2}$ and Bi 4f$_{7/2}$. The gap between both peaks is 5.3 eV, which suggests Bi^{3+} ions in the BHFO thin films [30]. Usually, the formation of Fe^{2+} ions will introduce oxygen vacancies to maintain charge balance. Therefore, it is considered that the existence of Fe^{2+} ions is a signal for oxygen vacancy presence. Equations (3) and (4) indicate the possible mechanism of oxygen vacancies and Fe^{2+} ions, as shown in Reference [31]:

$$Fe_2O_3 \Leftrightarrow 2Fe_{Fe}^x + 3O_O^x + 2V_{Bi}''' + 3V_O^{\bullet\bullet} \tag{3}$$

$$2Fe \Leftrightarrow 2Fe_{Fe}' + 2O_O^x + V_O^{\bullet\bullet} \tag{4}$$

In our results, Fe 2p peak separates into Fe 2p$_{3/2}$ and Fe 2p$_{1/2}$ spin–orbit doublets are seen at 723.8 eV and 710.8 eV. It can be identified as Fe^{3+}. It can be explained directly by the following equations [32]:

$$2Bi^{3+} + Ho^{3+} + 3O^{2-} \leftrightarrow Bi_2O_3 + Ho^{4+} + V_{Bi}''' + V_O^{\bullet\bullet} \tag{5}$$

$$Ho^{4+} + Fe^{2+} \leftrightarrow Fe^{3+} + Ho^{3+} \tag{6}$$

This means that the Fe ions in the BHFO thin film are positive trivalent, indicating that Ho doping inhibits the formation of Fe^{2+} ions. This confirms that the Ho^{3+} ion doping helps to suppress the Fe ion from Fe^{3+} to the Fe^{2+} and proves the reduction of oxygen vacancies in BHFO thin film [33, 34]. Moreover, this can further demonstrate the synthesized BHFO thin film which is in the unmixed phase. The peaks of O 1 s are located at 529.3 and 531.4 eV. And Ho 4d5/2 and Ho 4d peaks

are located at 163.8 and 158.5 eV. In this system, the Ho^{3+} ions will participate in enhancing ferromagnetism.

3.4 VSM Analysis

Figure 6 a shows the magnetic hysteresis loops (M-H) for BFO and BHFO thin films, where the remanent magnetization (Mr) and saturated magnetization (Ms) are observed in Fig. 6(b). The Mr and Ms of the BHFO thin films are 5.5 and 45.2 emu/cm2, respectively. The magnetization (Mr, Ms) in the BHFO thin film is observed to increase as compared with the BFO thin film. Observed magnetic behavior in BHFO thin films may have a number of contributions. According to reports, three possible reasons can explain the weak ferromagnetism in BHFO thin films. Firstly, the increase in magnetization of the BHFO might be due to the
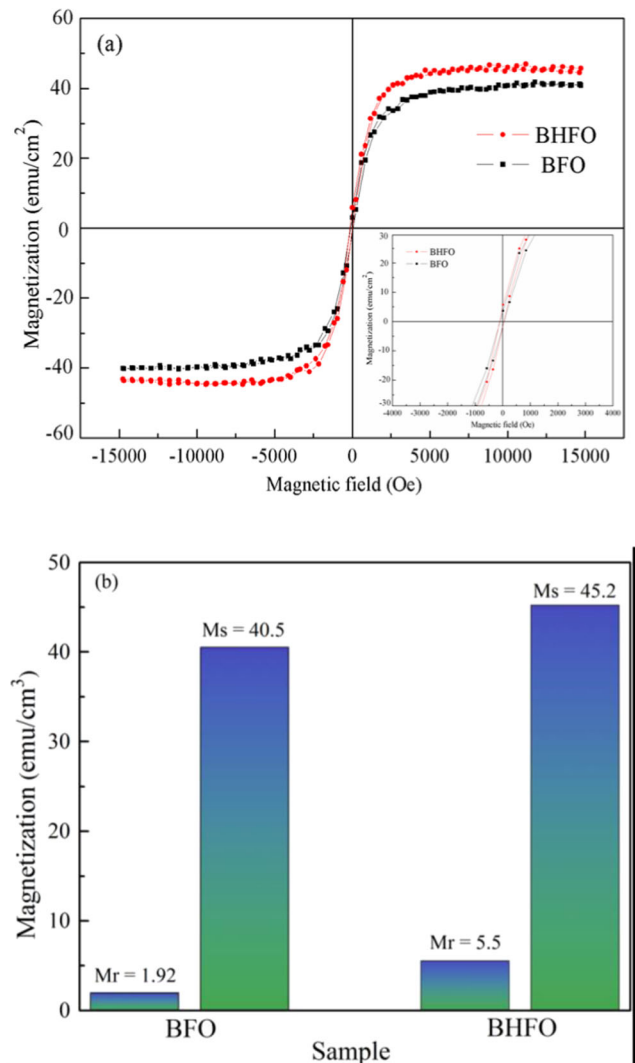

Fig. 6 (a) Magnetic field-dependent magnetization at room temperature for BFO and BHFO thin films; Inset shows the enlarged magnetization behavior of all thin films. (b) The magnetization value of the both thin films

destruction of the spin cycloid caused by the substitution of Ho ions, and the large deformation of the crystal structure due to the Ho ion exchange caused by large ionic different between Bi^{3+} and Ho^{3+} [35, 36]. Secondly, the average grain size of BFO and BHFO films listed in Table 1 is less than 62 nm. This is why BFO films exhibit weak ferromagnetism rather than antiferromagnetism at room temperature. This also is a reason why BFO thin films exhibit weak ferromagnetic property rather than antiferromagnetic property at room temperature [37]. This result is consistent with XRD analysis. Moreover, Ho^{3+} ion is a kind of magnetically active ion with a large magnetic moment. The third probable reason for the improvement of BHFO thin film may be Ho doping may have a high value of magnetization in comparison with other rare earth doped BHFO due to Ho-Ho and Ho-Fe couplings [38].

4 Conclusions

In conclusion, pure BFO and BHFO thin films are formulated on Si (100) substrates using a spin-coating processing. XRD, TEM, and SEM results demonstrate that all thin films possess a pristine phase and uniform surface morphology. Raman spectroscopy indicates that Ho successfully replaced the Bi site in BHFO thin films. Moreover, a crystal structure transformation is observed in BHFO thin film. The result of XPS analysis in the BHFO thin films can be identified as Fe^{3+}. Moreover, this can further demonstrate that the synthesized BHFO thin films are in the pure phase. Our magnetization measurement results show that the Ms of BHFO thin films are higher than that of the BFO thin films. The enhancement of magnetic properties can be associated with the destroyed spin cycloid, the average grain sizes less than 62 nm, and the Ho-Ho and Ho-Fe couplings.

References

1. Shirolkar, M.M., Li, J.N., Dong, X.L., Li, M., Wang, H.Q.: Controlling the ferroelectric and resistive switching properties of a BiFeO₃ thin film prepared using sub-5 nm dimension nanoparticles. Phys Chem Chem Phys. **19**, 26085 (2017)
2. Eerenstein, W., Mathur, N.D., Scott, J.F.: Multiferroic and magnetoelectric materials. Nature. **44**, 37 (2010)
3. Cheong, S.W., Mostovoy, M.: Multiferroics: a magnetic twist for ferroelectricity. Nat Mater. **6**, 13 (2007)
4. Catalan, G., Scott, J.F.: Physics and applications of bismuth ferrite. Adv Mater. **21**, 2463 (2010)
5. Zhang, Y.L., Wang, Y.H., Qi, J., Tian, Y., Sun, M.J., Zhang, J.K., Hu, T.J., Wei, M.B., Liu, Y.Q., Yang, J.H.: Enhanced magnetic properties of BiFeO₃ thin films by doping: analysis of structure and morphology. Nanomater. **8**, 711 (2018)
6. Damodaran, A.R., Liang, C.W., He, Q., Peng, C.Y., Chang, L., Chu, Y.H., Martin, L.W.: Nanoscale structure and mechanism for enhanced electromechanical response of highly strained BiFeO₃ thin films. Adv Mater. **23**, 3170 (2011)
7. Azizi, Z.S., Tehranchi, M.M., Hamidi, S.M., Vakili, S.H., Poormahdian, S.: Thermoelastic-tunable magnetic response of BiFeO\r, 3\r thin film on colloidal photonic crystal substrate fabricated by pulsed laser deposition. Phys Status Solidi A. **214**, 1 (2016)
8. Rana, D.S., Takahashi, K., Mavani, K.R., Kawayama, I., Murakami, H., Tonouchi, M., Yanagida, T., Tanaka, H., Kawai, T.: Implications of phase-segregation on structure, terahertz emission and magnetization of Bi(Fe₁₋ₓMnₓ)O₃ (0≤x≤0.5) thin films. Phys Rev B. **75**, 060405 (2007)
9. Liu, S.Y., Jiang, G.J., Liu, G.S., Li, W.J., Xing, J.J.: Effects of Nd, Al doping on the structure and properties of BiFeO₃. J Supercond Nov Magn. **21**, 2463 (2009)
10. Zhang, Y.L., Qi, J., Wang, Y.H., Tian, Y., Zhang, J.K., Hu, T.J., Wei, M.B., Liu, Y.Q., Yang, J.H.: Tuning magnetic properties of BiFeO₃ thin films by controlling Mn doping concentration. Ceram Int. **44**, 6054 (2017)
11. Hur, N., Park, S., Sharma, P.A., Ahn, J.S., Guha, S., Cheong, S.W.: Electric polarization reversal and memory in a multiferroic material induced by magnetic fields. Nature. **429**, 392 (2004)
12. Liu, H.J., Liang, C.W., Liang, W.I., Chen, H.J., Yang, J.C., Peng, C.Y., Wang, G.F., Chu, F.N., Chen, Y.C., Lee, H.Y., Chang, L., Lin, S.J., Chu, Y.H.: Strain-driven phase boundaries in BiFeO₃ thin films studied by atomic force microscopy and x-ray diffraction. Phys Rev B. **85**(014104), (2012)
13. Liu, Y.Q., Wang, Y.H., Li, D., Zhang, Y.J., Zhang, J., Yang, J.H.: A study of structural, ferroelectric, ferromagnetic, dielectric properties of NiFe₂O₄-BaTiO₃ multiferroic composites. J Mater Sci Mater Electron. **24**, 1900 (2013)
14. Titus, S., Srinivasu, V.V., Balakumar, S., Sakar, M., Das, J.: Electron spin resonance studies of undoped and dysprosium doped bismuth ferrite nanoparticles. J Supercond Nov Magn. **30**, 819 (2017)
15. Wang, L.C., Wang, Z.H., He, S.L., Li, X., Lin, P.T., Sun, J.R., Shen, B.G.: Enhanced magnetization and suppressed current leakage in BiFeO3 ceramics prepared by spark plasma sintering of sol-gel derived nanoparticles. Physica B. **407**, 1196 (2012)
16. Bai, Z.L., Cheng, X.X., Chen, D.F., Zhang, D.W., Chen, L.Q., Scott, J.F., Hwang, C.S., Jiang, A.Q.: Hierarchical domain structure and extremely large wall current in epitaxial BiFeO₃ thin films. Adv Funct Mater. **28**, 1801725 (2018)
17. Liu, Y.Q., Qi, J., Zhang, Y.L., Wang, Y.H., Feng, M., Zhang, J.K., Wei, M.B., Yang, J.H.: Surface agglomeration is beneficial for release of magnetic property via research of rare earth (RE) element-substitution. Appl Surf Sci. **427**, 745 (2018)
18. Radheshyam, R., Sunil, K.M., Singh, N.K., Seema, S., KAndrei, L.: Preparation, structures, and multiferroic properties of single-phase BiRFeO₃, R = La and Er ceramics. Curr Appl Phys. **11**, 508 (2011)
19. Rana, D.S., Takahashi, K., Mavani, K.R., Kawayama, I., Murakami, H., Tonouchi, M., Yanagida, T., Tanaka, H., Kawai, T.: Thickness dependence of the structure and magnetization of BiFeO₃ thin films on (LaAlO₃)₀.₃(Sr₂AlTaO₆)₀.₇ (001) substrate. Phys Rev B. **75**, 060405 (2007)
20. Zheng, Y.J., Tan, G.Q., Ren, H.J., Xia, A.: A kind of Bi₁₋ₓErₓFeO₃ films with potential excellent multiferroic performances. J Mater Sci. **52**, 4903 (2007)
21. Betancourt-Cantera, L.G., Bolarín-Miró, A.M., Cortés-Escobedo, C.A., Hernández-Cruz, L.E., Sánchez-De Jesús, F.: Structural

transitions and multiferroic properties of high Ni-doped $BiFeO_3$. J Magn Magn Mater. **456**, 381 (2018)

22. Khajonrit, J., Wongpratat, U., Kidkhunthod, P., Pinitsoontorn, S., Maensiri, S.: Effects of Co doping on magnetic and electrochemical properties of $BiFeO_3$ nanoparticles. J Magn Magn Mater. **449**, 423 (2018)

23. Yu, L., Deng, H.M., Zhou, W.L., Zhang, Q., Yang, P.X., Chu, J.H.: Effects of (Sm, Mn and Ni) co-doping on structural, optical and magnetic properties of $BiFeO_3$ thin films fabricated by a sol-gel technique. Mater Lett. **170**, 85 (2016)

24. Godara, P., Agarwal, A., Ahlawat, N., Sanghi, S., Dahiya, R.: Crystal structure transformation, dielectric and magnetic properties of Ba and Co modified $BiFeO_3$ multiferroic. J Alloys Compd. **594**, 175 (2014)

25. Li, Z.J., Hou, Z.L., Song, W.L., Liu, X.D., Cao, W.Q., Shao, X.H., Cao, M.S.: Unusual continuous dual absorption peaks in Ca-doped $BiFeO_3$ nanostructures for broadened microwave absorption. Nanoscale. **8**, 10415 (2016)

26. Surbhi, G., Monika, T., Vinay, G.: Raman spectroscopy of nanocrystalline Mn-doped $BiFeO_3$ thin films. J Exp Nanosci. **8**, 261 (2013)

27. Dimitrij, S., Milena, R., Petronijević, N., Tasić, N., Branko, M., Biljana, S.: Dielectric and ferroelectric properties of ho-doped $BiFeO_3$ nanopowders across the structural phase transition. Ceram Int. **43**, 16531 (2017)

28. Yuan, G.L., Or, S.W., Chan, H.L.W., Liu, Z.G.: Reduced ferroelectric coercivity in multiferroic $Bi_{0.825}Nd_{0.175}FeO_3$ thin film. J Appl Phys. **101**, 024106 (2007)

29. Liu, Y.Q., Zhang, J., Wu, Y.H., Zhang, Y.J., Wei, M.B., Yang, J.H.: Enhancement of magnetization in Er doped $BiFeO_3$ thin film. J Sol-Gel Sci Technol. **67**(1), 1 (2013)

30. Yoneda, Y., Kitanaka, Y., Noguchi, Y., Miyayama, M.: Electronic and local structures of Mn-doped $BiFeO_3$ crystals. Phys Rev B. **86**, 184122 (2012)

31. Raghavan, C.M., Kim, J.W., Kim, S.S.: Structural and electrical properties of $(Bi_{0.9}Dy_{0.1})(Fe_{0.975}TM_{0.025})O_{3\pm\delta}$ (TM=Ni^{2+}, Cr^{3+} and Ti^{4+}) thin films. Ceram Int. **39**, 3563 (2013)

32. Karpinsky, D.V., Troyanchuk, I.O., Willinger, M., Khomchenko, V.A., Salak, A.N., Sikolenko, V., Silibin, M.V.: Intermediate structural state in $Bi_{1-x}Pr_xFeO_3$ ceramics at the rhombohedral-orthorhombic phase boundary. J Mater Sci. **52**, 9355 (2017)

33. Qi, J., Zhang, Y.L., Wang, Y.H., Liu, Y.Q., Wei, M.B., Zhang, J.K., Feng, M., Yang, J.H.: Effect of Cr doping on the phase structure, surface appearance and magnetic property of $BiFeO_3$ thin films prepared via sol-gel technology. J Mater Sci Mater Electron. **28**, 17490 (2017)

34. Jin, J., Zheng, C.H., Yang, H.M.: Natural diatomite modified as novel hydrogen storage material. Funct Mater Lett. **07**, 1450027 (2014)

35. Yao, W., Nan, C.W.: Enhanced ferroelectricity in Ti-doped multiferroic $BiFeO_3$ thin films. Appl Phys Lett. **89**, 052903 (2006)

36. Islam, M.R., Islam, M.S., Zubair, M.A., Usama, H.M., Azam, M.S., Sharif, A.: Correlation of charge defects and morphology with magnetic and electrical properties of Sr and Ta codoped $BiFeO_3$. J Alloys Compd. **735**, 2584 (2018)

37. Park, T.J., Papaefthymiou, G.C., Viescas, A.J., Moodenbaugh, A.R., Wong, S.S.: Size-dependent magnetic properties of single-crystalline multiferroic $BiFeO_3$ nanoparticles. Nano Lett. **7**, 766 (2007)

38. Singh, J., Agarwal, A., Sanghi, S., Bhasin, T., Yadav, M., Bhakar, U., Singh, O.: Effect of Ba and Ho co-doping on crystal structure, phase transformation, magnetic properties and dielectric properties of $BiFeO_3$. Curr Appl Phys. **19**, 321 (2019)